# 5. Temporal constraints for unstable slip – $^{40}Ar/^{39}Ar$ geochronology applied to pseudotachylytes


## Abstract

$^{40}Ar/^{39}Ar$ isotopic data obtained by stepwise heating using a laser system from pseudotachylytes occurring in the basal parts of the Austroalpine domain in the northwestern part of the Engadine window constrain the timing of unstable slip within the seismogenic zone of a fossil convergent plate interface zone. Formation of pseudotachylyte as unambiguous evidence for fossil seismicity is dated to have occurred during a time span between 60 Ma to 80 Ma. This corroborates previous data obtained by Thöni (1981, 1988). However, the heterogeneous texture of the ultra fine grained pseudotachylyte groundmass, most likely composed of a mixture of amphibole, feldspar and biotite (obtained by defocused beam microprobe bulk analyses), as well as the incorporation of host rock material of comparable size (rock fragments and single minerals) complicate the interpretation of the isotopic data. Therefore, the Ca/K ratio provides first roughly indications for the degassing of material enriched in Ca, most probable the inherited host rock material. Due to the temporal similarity between age data for higher pressure metamorphism of South Penninic and Austroalpine rocks and pseudotachylyte formation, and the fact that the pseudotachylytes occur subparallel (i.e. slightly discordant) to the main thrust, we interpret the generation of pseudotachylytes to be related to unstable slip processes occurring along the plate interface zone during the course of subduction of the South Penninic ocean underneath the Austroalpine upper plate.


## 5.1. Introduction

Unstable slip in the upper part of active convergent plate margins occurs within a limited depth range along the plate interface, typically between 5 km and 45 km depth (so-called seismogenic coupling zone, e.g. Ruff and Kanamori 1983, Tichelaar and Ruff 1993), causing major interplate earthquakes. Until now, the plate interface of convergent plate boundaries cannot be directly accessed. Hence, direct investigations of exhumed ancient convergent plate boundaries are requested to achieve insights into deformation processes occurring along the plate interface despite multiple overprinting during exhumation. We use the exposure of a former plate interface in the European Alps, one of the best-studied mountain belts that has resulted from successive subduction, accretion and collision (Froitzheim et al., 1994; Handy, 1996; Schmid et al., 1996; Pfiffner et al., 2000) to address the question of timing of unstable slip. Therefore, we analyzed pseudotachylytes from the basal parts of the upper plate immediately above a subduction mélange at the northwestern rim of the Engadine window. This suture traces the plate interface zone of a fossil convergent plate margin.

Pseudotachylytes as evidence for unstable slip are the field record of paleoseismic events occurring in the seismogenic zone of large scale crustal faults (e.g. Sibson 1975). Adopting this assumption for

exhumed ancient subduction plate interfaces, the presence of pseudotachylytes constrains the depth range of the exposed fossil counterpart to be situated within the former seismogenic coupling zone. Due to the presence of pseudotachylytes, the here presented study contributes to the understanding of convergent plate interfaces in the depth range of their former seismogenic zone. We shed light on the timing of unstable slip with the help of $^{40}Ar/^{39}Ar$ geochronology applied to the pseudotachylytes. As recommended by Müller et al. (2002), we used stepwise heating with a laser system until total fusion for gas release. According to Maddock (1992) we applied microprobe analyses with a defocused beam to study the bulk composition of the ultra fine grained pseudotachylyte groundmass.

## 5.2. Geological, metamorphical, and structural framework of the working area

The European Alps resulted from collision of the European and the Adriatic continental plates and southeastward to southward subduction and accretion of the intervening Penninic oceanic domain. The Penninic domain consists of two oceanic basins related to the Alpine Tethys (North Penninic Valais basin and South Penninic ocean), divided by the so-called Briançonnais continental swell (Middle Penninic) (e.g. Florineth and Froitzheim 1994, and references therein). These units were successively subducted and accreted to the base of the Adriatic plate (Austroalpine domain in the working area) since the Late Cretaceous until the final collision of the Adriatic plate with the European plate during the Middle Tertiary.

The working area is located at the northwestern rim of the Engadine window (Figs. 5.1, 5.2). The main geological units are represented by the South Penninic and Austroalpine domain. The South Penninic domain forms a tectonic subduction mélange caused by the Late Cretaceous to Eocene subduction of the South Penninic ocean underneath the Austroalpine upper plate. This mélange zone is composed of intensely deformed oceanic and continental material (Deutsch 1983, Ring et al. 1988, and references therein) comprising Jurassic ophiolites, radiolarian chert, pelagic limestone, shale and sandstone (Ring et al. 1988). Competent blocks of Austroalpine and Penninic affinity are embedded in the incompetent shaly matrix (Ring et al. 1990). The large-scale structures of the whole South Penninic mélange are construed by e.g. Ring et al. (1988, 1989, 1990) as the deep parts of an accretionary wedge formed at the tip of and below a thrust belt migrating towards the west. The Austroalpine upper plate consists of a suite of gneissic to amphibolitic, mainly upper crustal rocks, which experienced pre-Alpine (mainly Permo-Carboniferous) and Early (Eo-) Alpine deformation (e.g. Florineth and Froitzheim 1994, Manatschal et al. 2003, Ring et al. 1988). Metamorphic conditions of South Penninic rocks in the working area are in the range from lower greenschist facies to middle greenschist facies. The Austroalpine domain was metamorphosed to lower greenschist facies conditions during Alpine deformation in the working area (e.g. Handy and Oberhänsli 2004).

The South Penninic subduction mélange close to the contact to the Austroalpine upper plate experienced a penetrative deformation with an inferred top-W direction of tectonic transport (see Chapter 4, e.g. Bachmann et al. submitted). Deformation with general top-W directed tectonic transport of the Austroalpine nappe stack is expressed by microscale fracture zones reactivating the preexisting foliation of probably Variscan age. Orientation of these fracture zones and the preexisting foliation in the Austroalpine rocks parallels the corresponding foliation

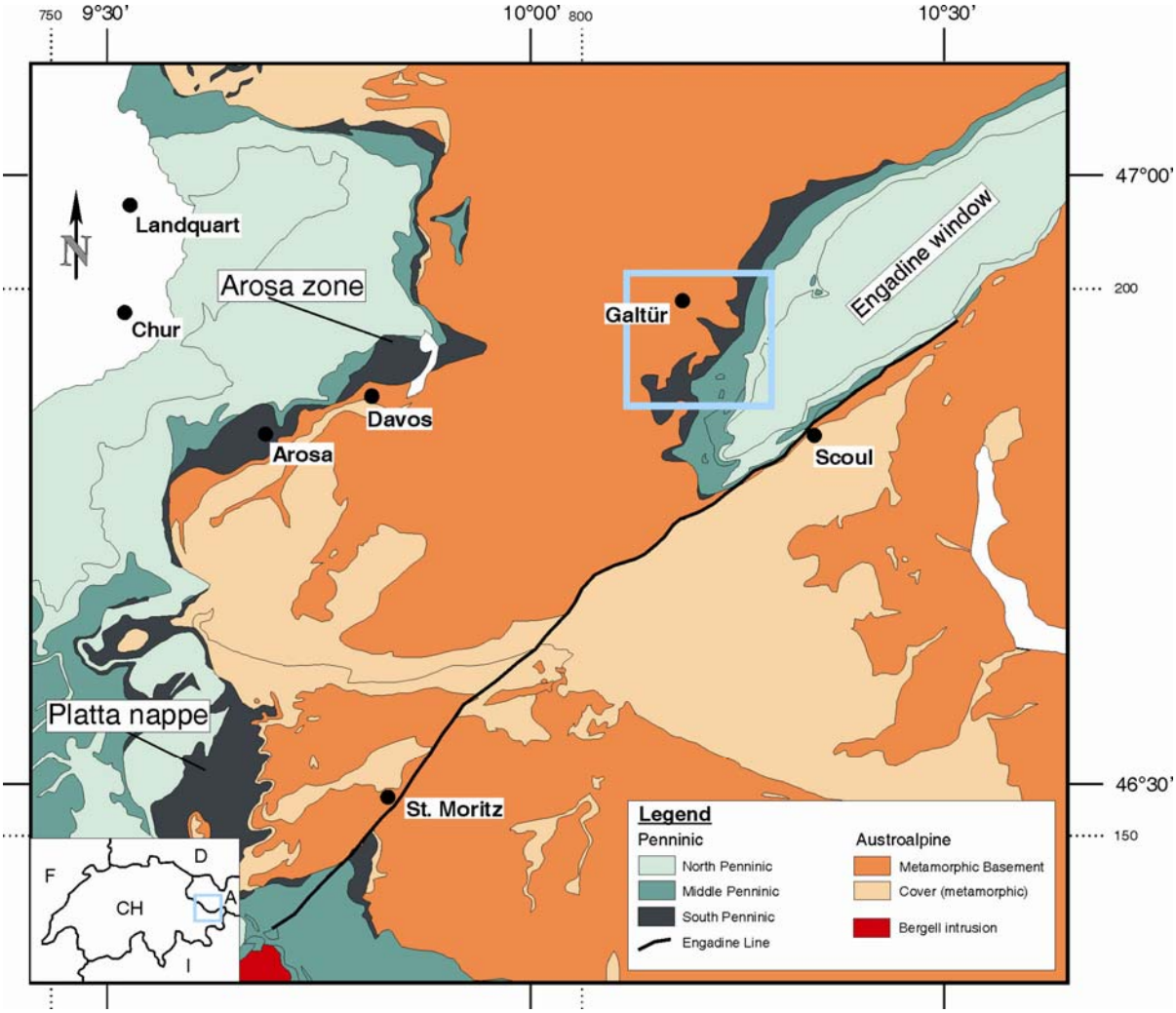


Figure 5.1: Geological map of the study area emphasizing the suture zone between the South Penninic (dark green) and the Austroalpine (orange, part of the Adriatic plate). Arosa zone and Platta nappe are local names for rocks of South Penninic affinity. Based on the Tectonic map of Switzerland 1:500.000, 2nd edition (1980). Blue rectangle emphasizes the working area located at the northwestern rim of the Engadine window.

within the South Penninic mélange, at least in the first few hundred meters above the base of the hanging wall. In general, orientation of structural data and the therewith assessed direction of tectonic transport are similar in both the South Penninic mélange and the basal parts of the Austroalpine upper plate. This is also the case for their metamorphic conditions reached during Alpine deformation. Subsequent localized deformation with significant lower intensity overprints the top-W structures, but a complete erasure of the top-W structures in both the South Penninic mélange and the Austroalpine nappes by younger deformational processes cannot be observed (see also Ring 1989, Dürr 1992).

The boundary between the South Penninic mélange in the footwall and the Austroalpine upper plate in the hanging wall represents a large scale thrust zone, where Austroalpine rocks were thrusted onto the South Penninic mélange. The most prominent feature within the study area are pseudotachylytes, which occur in the first ~300 m above the base of the upper plate, which are previously described by a number of authors (e.g.

Gürler and Schmutz 1995, Masch 1970, 1974, Koch and Masch 1992, Thöni 1988). The frequency of these brittle fault rocks decreases with increasing distance from the base of the upper plate. Therefore, they are supposed to be related to the emplacement of the Austoralpine nappe stack onto the South Penninic domain (e.g. Gürler and Schmutz 1995). Pseudotachylytes occur both concordant and discordant to the preexisting layering, preferentially formed along lithological boundaries. Pseudotachylytes occur slightly discordant to the main thrust fault (Gürler and Schmutz 1995). However, we never recognized pseudotachylytes within metasedimentary rocks of the South Penninic mélange, neither in the matrix nor in the clasts.

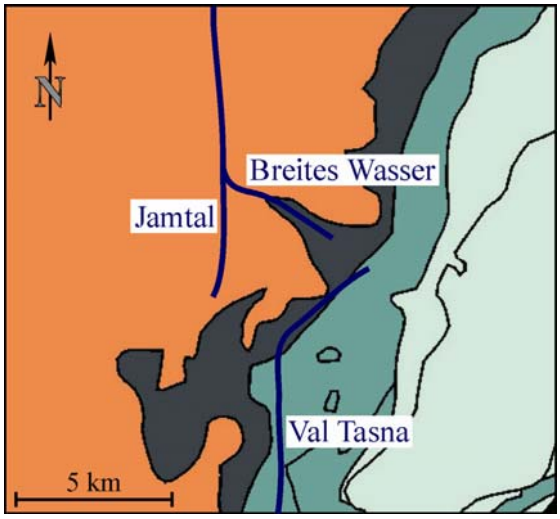


Figure 5.2: Close-up of the working area indicating the sampling areas Jamtal valley, valley Breites Wasser, and valley Val Tasna. Close-up equals blue rectangle in Figure 5.1. For explanation of signatures see legend in Figure 5.1.

Additionally, we observed an overprint of pseudotachylytes by viscous deformation, maybe promoted by the small grain size of the recrystallized pseudotachylytes favoring viscous grain-size sensitive deformation mechanisms (grain boundary sliding) (see Chapter 4). This overprint is most prominent just above the main thrust plane. The wall rock hosting the pseudotachylytes (Austroalpine basement) does not exhibit an Alpine mylonitic overprint. Mylonitic deformation is rather assigned to the higher grade amphibolite facies metamorphism during Variscian orogeny (due to the mineral composition of the mylonitic rocks) (Schmutz 1995), a metamorphic grade, which was not reached during Alpine orogeny. Moreover, there is a mutual crosscutting relationship between undeformed pseudotachylytes and mylonitized pseudotachylytes pointing to spatiotemporal changes of brittle and viscous deformation.

## 5.3. Pseudotachylytes – General information

The term “pseudotachylyte” was originally introduced by Shand (1916) due to the resemblance of dark veins in the Vredefort area (South Africa) to tachylytes, which represent mafic volcanic glass. Today, pseudotachylytes describe cohesive glassy or very fine grained brittle fault rocks. According to Cowan (1999), they are the only unambiguous evidence for deformation at seismic velocity ($\geq$ 1 m/s). Pseudotachylytes represent melt veins due to frictional heating produced by sliding (e.g. Sibson 1975, Spray 1987). In addition, Wenk (1978) proposed that pseudotachylytes result from fluidization of material due to frictional-induced ultracataclasis, rather than from friction-induced melting. According to results from high-speed slip experiments conducted by Spray (1995), comminution by ultracataclasis and frictional melting may take place in fully transitional stages, not explicitly excluding each other. However, both require high deformation rates. Therefore, pseudotachylytes are thought to be associated with either hyper-velocity impact events, or high-velocity coseismic slip along crustal fault zones (Spray 1992). Additionally, pseudotachylytes are reported to have been produced at the base of large landslides (Legros et al. 2000).

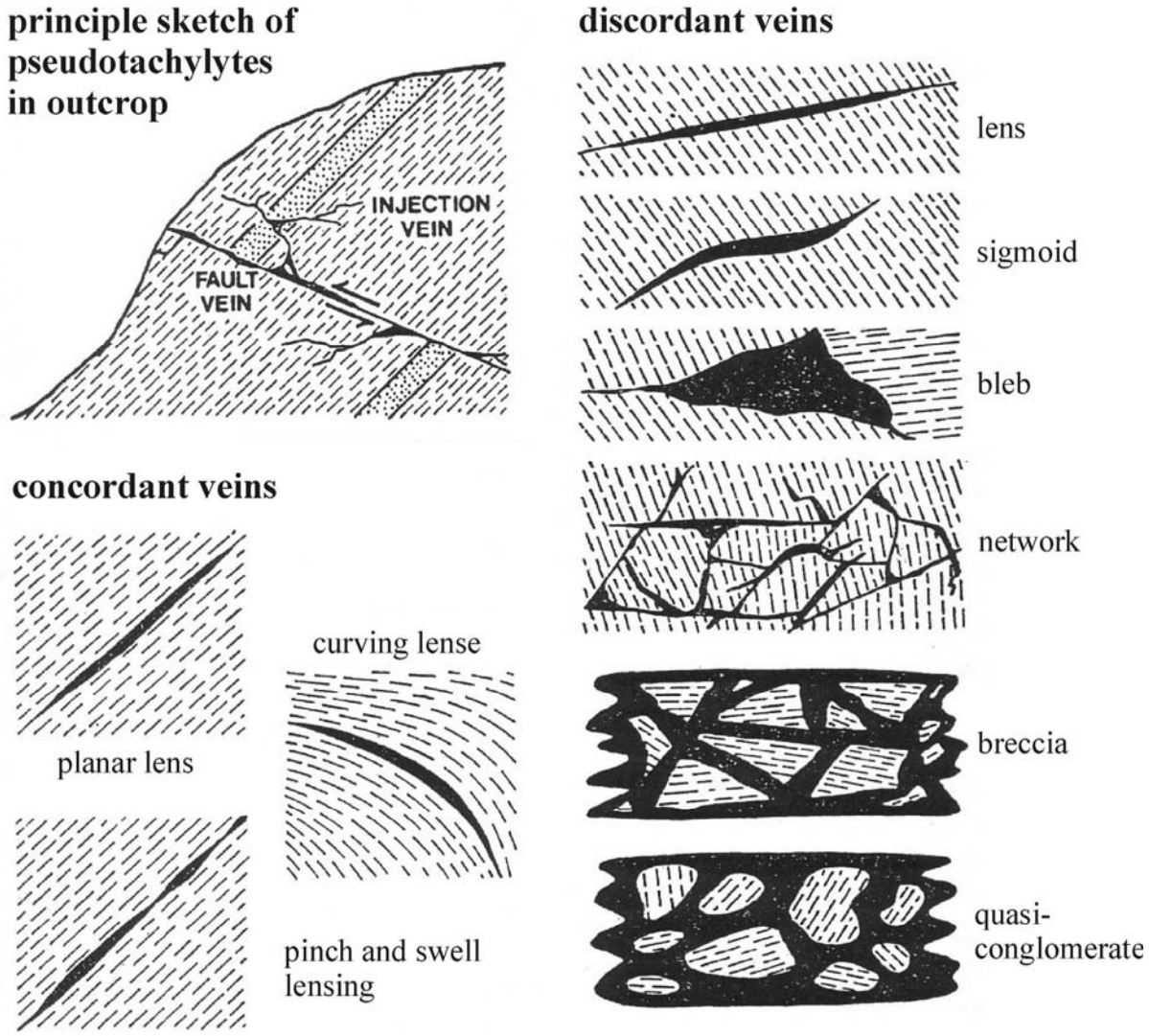


Figure 5.3: Principle drawing of main pseudotachylyte geometries and textures. Modified after Sibson (1975).

In general, pseudotachylytes form along so-called generation surfaces (fault veins, Fig. 5.3). Veins inject into the host rock with a high angle (roughly 90°) to this main surface (injection veins, Fig. 5.3) (Sibson 1975). Fault veins are situated along planar shear fractures, whereas injection veins represent tensile fractures and voids, in which the melt was squeezed-off from the generation surface (e.g. Sibson 1975). According to e.g. Sibson (1975) other key geometric characteristics are: sharp boundaries to the host rock, and a dark matrix with mineral and wall rock fragments. Pseudotachylytes occur as networks, layers or form the matrix of breccia zones (Figs. 5.3, 5.4). They are oriented concordant or discordant to a pre-existing layering, but they are preferentially formed along lithological contrasts (e.g. Kenkmann et al. 2000).

Formation of pseudotachylytes occurs mainly in dry and low porosity rocks. Fluids would prevent the built-up of high effective normal stress and associated shear stress by ongoing hydraulic fracturing, hence cause a lower potential for shear heating. In contrast, dry crystalline rocks support higher effective normal stress and associated shear stress, a prerequisite for the formation of shear

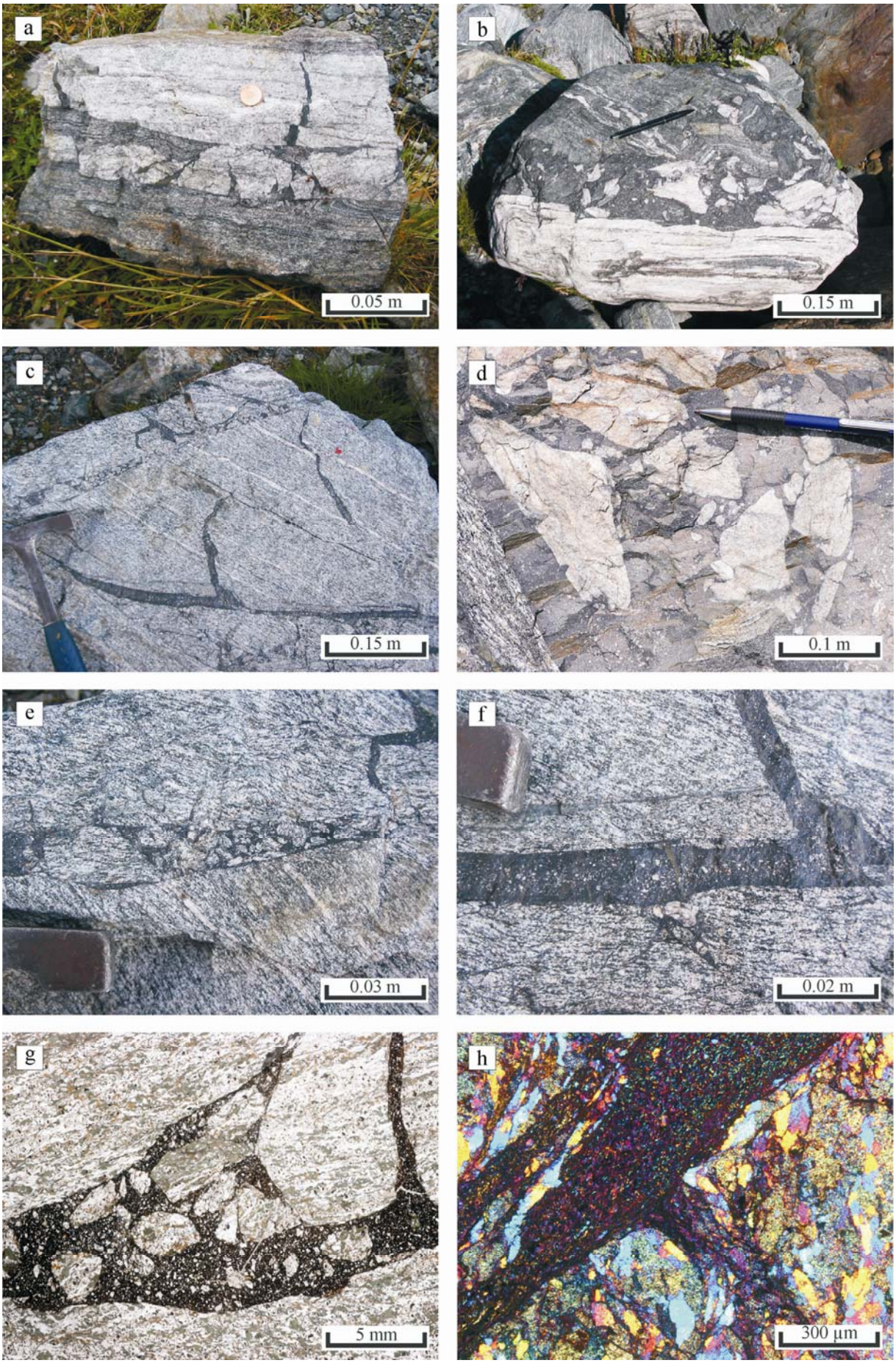
a
0.05 m
b
0.15 m
c
0.15 m
d
0.1 m
e
0.03 m
f
0.02 m
g
5 mm
h
300 µm

Figure 5.4: Outcrop and thin section images of pseudotachylytes from the northwestern rim of the Engadine window. a) pseudotachylyte exhibiting a ladder network, b) pseudotachylyte forming the matrix of a breccia zone, c) pseudotachylyte with fault vein and injection vein (~90° from the main surface), d) pseudotachylyte with embedded wall rock fragments of different size, e) pseudotachylyte exhibiting a large number of wall rock fragments. Note the sharp boundaries to the wall rock, f) pseudotachylyte with only small fragments from the host rock, aligned within the center of the pseudotachylyte, most likely due to flow processes, g) scanned thin section showing wall rock fragments of different size embedded in the dark ultra fine grained pseudotachylyte matrix, and h) thin section image (with λ-filter) of pseudotachylyte with injection vein.

fractures and frictional heating, and thus for pseudotachylytes. Melting temperatures are inferred from the absence of host rock minerals as inclusions within the ultra fine grained pseudotachylyte matrix. Therefore, temperatures between 750°C (melting of biotite, muscovite) up to 1600°C (melting of high-Ca-feldspar, quartz) are predicted on the main fault (Spray 1992). In consequence, there is a preferred melting of Fe-Mg-Al silicates, which are almost completely absent as mineral inclusions in the pseudotachylyte matrix. Rapid quenching might lead to the crystallization of spherolites, which represents in composition the former melted paragenesis.

## 5.4. Published age data

Subduction of the South Penninic ocean initiated at around 120 Ma to 100 Ma (Handy and Oberhänsli 2004, and references therein). Pressure-dominated metamorphism in the Lower Austroalpine units occurred at around 90 Ma to 60 Ma, and in the South Penninic and European units at around 60 Ma to 35 Ma (Handy and Oberhänsli 2004, and references therein). Schmid et al. (2004) reported HP metamorphism of South Penninic rocks during the Tertiary, at least for the Western Alps. Handy and Oberhänsli (2004, and references therein) reported thrusting and accretion under HP-greenschist facies conditions during a time span between 88 Ma and 76 Ma for the Austroalpine domain to the south of our study area. These data show the migration of subduction related deformation towards the foreland, which finally culminated in the collision with the European margin.

The pseudotachylytes occurring along the northwestern margin of the Engadine window have been already dated by Thöni (1981, 1988) using K/Ar geochronology on whole rock pseudotachylyte samples and Rb/Sr geochronology with the thin slab method, respectively. The K/Ar method resulted in different age groups ranging between 53 Ma to 58 Ma, 73 Ma to 78 Ma, and 114 Ma. Thöni (1981) interpreted these ages to reflect Cretaceous pseudotachylyte formation at around 75 Ma. The younger ages should be caused by later thermal or tectonic processes favoring a loss of radiogenic Ar. The older age group is interpreted to be caused by the analyses of older clasts remained within the pseudotachylyte groundmass. The Rb/Sr analyses (Thöni 1988) resulted in two ages around 75 Ma. Together, both methods are thought to reflect pseudotachylyte formation at roughly 75 Ma along the base of the Austroalpine nappe stack.

## 5.5. Methods

We used different methods to shed light on the timing of unstable slip within the study area. At first, we analyzed the relevant samples with a petrographic microscope. Due to their ultra fine grain size (at least in the groundmass of the pseudotachylytes) we subsequently used scanning electron microscopy (SEM). Microprobe analyses were conducted to identify the bulk

composition of the pseudotachylyte groundmass and the embedded clasts.

Mineral analyses were performed using both a CAMECA SX100 electron microprobe operating in the wavelength-dispersive mode at the GFZ Potsdam and a JEOL JXA-8200 electron microscope at the FU Berlin. Major and minor elements were determined at 15 kV acceleration voltage and a beam current of 11 nA to 20 nA with counting times of 20 s for major elements, and 30 s for minor elements. The standard sets of the Smithsonian Institute (cf. Jarosewich et al. 1980) and of MAC™ were used for reference. In addition to focused beam analyses (beam diameter 1µm to 10 µm) we used defocused beams with a beam diameter ranging from 30 µm up to 100 µm. This variation was necessary due to differences in the internal structure of the samples regarding to size, concentration and distribution of embedded clasts in order to cover exclusively groundmass material. Microprobe analytical data are given in the appendix A. The JEOL JXA-8200 microprobe was additionally used to obtain back-scattered electron images (BSE). In addition, we used a DSM 962 scanning electron microscope (SEM) at the GFZ Potsdam to obtain secondary electron images (SE), as well as BSE images.

The study of Müller et al. (2002) pointed out that reliable results for pseudotachylyte formation ages can be best achieved using the $^{40}Ar/^{39}Ar$ method, both with stepwise heating or laser ablation. Therefore, we conducted $^{40}Ar/^{39}Ar$ geochronology with stepwise heating using a laser on pseudotachylytes from the northwestern part of the Engadine window to further constrain their formation ages, and to relate them to the overall geological evolution of the South Penninic-Austroalpine plate interface zone. Argon, which is expelled from the sample in the different temperature steps, was simultaneously measured in a mass spectrometer, and Ar isotopes were calculated for each step.

In an initial phase, we macroscopically selected pseudotachylytes, which appear to be undeformed and less altered. Petrographic microscopy was used the study the chosen samples in more detail in terms of amount and petrography of clasts embedded within the ultra fine grained pseudotachylyte matrix. Care was taken to exclude material altered by weathering or fluid-rock interaction. Afterwards, 300 µm thick slices of pseudotachylytes were produces and highly polished on both sides. Then, these slices were cut into small pieces of roughly 5 x 5 mm, and were checked using a binocular microscope to avoid embedded clasts, which would represent an error source for excess argon. Samples were washed in de-ionized water to remove fine powder on the surface of grains (health risk after irradiation). After washing, grains were dried in an oven at roughly 100°C.

For irradiation, samples were individually wrapped in Al foil and than packed into holes within a 99.999 % pure Al disk. Samples were irradiated for four days in a reactor at the GKSS Geesthacht. After the irradiated samples returned from the reactor, the Al foils were opened and the samples were recollected for subsequent argon isotope analyses. The grains were loaded into holes within a Cu disk. This disk was finally introduced into a vacuum line at the Ar laboratory of the University of Potsdam. We used an automated laser extraction and gas cleanup system operating with both a Merchantek LUV266X quadrupled laser emitting UV at 266 nm and a Merchantek floating MIR10IR ($CO_2$) (20W Nd-YAG) laser. These laser systems allow both in-situ ablation of small spots on the samples and bulk step-heating. After extraction of Ar gas from the sample by step heating (several steps until total fusion), the gas was purified in the ultra high vacuum

analytical line. Ar gas was introduced into a Micromass 5400 Static Vacuum Mass Spectrometer. Then, the isotopic ratios were obtained. Finally, obtained data were used to produce plateau and isochron plots, both normal and inverse. Ages were calculated using the Isoplot/Ex program of Ludwig (1999). The use of degassing steps to define a plateau age is defined in several ways, e.g. by a contiguous gas fraction comprising more than 50% of total $^{39}Ar$ released (Fleck et al. 1977), or by a sequence of five or more steps, where all data agree within 2σ error (Berger and York 1981). Analytical errors were applied within the calculation using weighted errors. Data point errors are 2σ standard deviation. Data of the different analyses are summarized in the appendix B.

## 5.6. Sampling and petrography

Throughout the working area (Figs. 5.1, 5.2) we sampled pseudotachylytes, which appeared macroscopically fresh and unaltered. They occur in veins of up to 20 cm width (Fig. 5.4). Freshness of samples was subsequently checked by using petrographical and binocular microscopes. In consequence, we selected five samples for further analyses. In general, the pseudotachylytes exhibit a dark ultra fine grained groundmass with embedded clasts, both comprising wall rock fragments and single minerals, mostly quartz and minor feldspar (Fig. 5.4). Description of the samples is organized geographically; first introducing samples from the Jamtal, followed by the Val Tasna, and the valley Breites Wasser (Fig. 5.2).

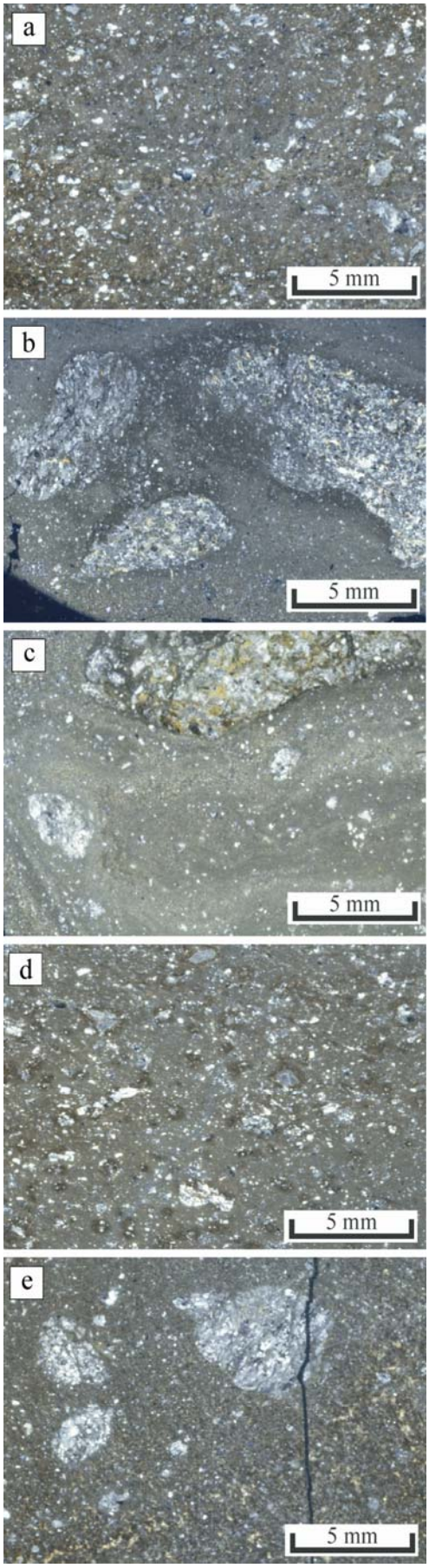


Figure 5.5: Scanned thin sections of samples used for $^{40}Ar/^{39}Ar$ geochronology. a) sample 1b, b) sample 5, c) sample 16, d) sample J96-1, and e) sample J96-2. See text for details.

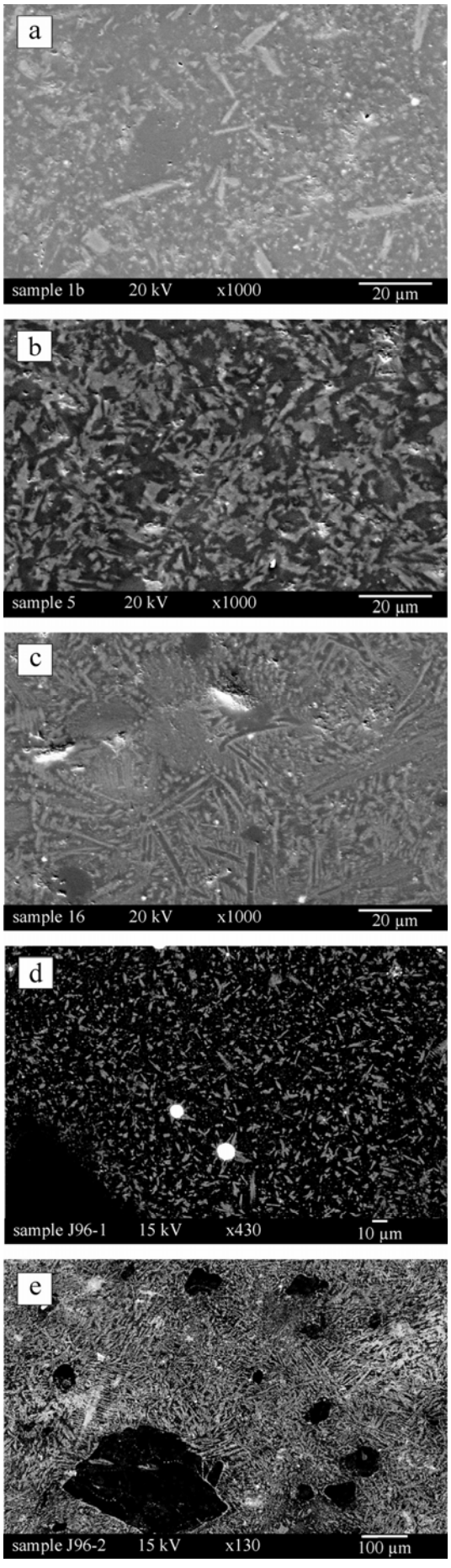


Figure 5.6: BSE and SE images obtained by microprobe and SEM of samples used for $^{40}Ar/^{39}Ar$ geochronology. a) sample 1b, b) sample 5, c) sample 16, d) sample J96-1, and e) sample J96-2. See text for details. Acceleration voltage is 15 kV and 20 kV, respectively. Magnification is 130, 430, and 1000, respectively.

Sample 1b represents a pseudotachylyte taken from the basal parts of the Austroalpine upper plate at the northwestern rim of the Engadine window in the Jamtal valley (Fig. 5.2). On a macroscopic scale, the pseudotachylyte appears to be dark with only minor inclusions within a dense matrix. On a microscopic scale, the sample exhibits a large number of small inclusions of both wall rock fragments and single minerals (Fig. 5.5a). While using 300 µm thin polished slices and a binocular microscope we avoided to probe these clasts. The SE image obtained by the SEM shows small lasts of only 20 µm length comprising the dense ultra fine grained groundmass (Fig. 5.6a). A microprobe analyses of its bulk composition exhibits roughly 60 mole-% $SiO_2$, 19 mole-% $Al_2O_3$, 7 mole-% FeO, and minor amounts of $TiO_2$, MgO, CaO, $Na_2O$ and $K_2O$. This might point to a mixture between amphibole and feldspar, both reflecting the paragenesis of the host gneisses.

Sample 5 is a pseudotachylyte sampled in the Val Tasna (NW part of Engadine window, Fig. 5.2). Macroscopically, it exhibits a dark and dense groundmass with large wall rock fragments. A few single mineral inclusions are visible. Microscopically, an ultra fine grained matrix with minor inclusions, smaller in comparison to sample 1b, and some large wall rock fragment are visible (Fig. 5.5b). The BSE image of the matrix shows the growth of very small (a few µm thick) lasts of single crystals (Fig. 5.6b). The bulk microprobe analysis points again to a possible mixture between amphibole and

feldspar. Here, the groundmass is enriched in Ca.
Sample 16 represents a pseudotachylyte from the Val Tasna in the northwestern part of the Engadine window (Fig. 5.2). The macroscopic dark and dense matrix contains small wall rock fragments, and single minerals. A few larger fragments from the host gneiss are also visible. This is also reflected in the microscopic view. In addition, flow textures from the primary melting stage might be present (Fig. 5.5c). The BSE image exhibits needles and partly spherolites, approved signs for crystallization from a melt (Fig. 5.6c). Bulk analysis points to a mixture of amphibole and feldspar as well. The groundmass is enriched in FeO compared to the previous analyzed samples.
J96-1 is a pseudotachylyte sample taken from the valley Breites Wasser, a side valley of the Jamtal (Fig. 5.2). This sample originates about 20 m above the main thrust plane. The host rock is an amphibole bearing layered gneiss. On the macroscopic scale, the matrix is dense and dark. Only a few inclusions of both wall rock fragments and single minerals are visible. This is also valid for the microscopic scale. There, the matrix exhibits parts with less frequent wall rock fragments and single minerals (Fig. 5.5d). These areas were subsequently used for further preparation. The BSE image shows ultra fine grained needles within the matrix. Partly, these needles form dendritic and spherolitic structures starting to growth on clast surfaces. In addition, sulfide droplets are visible within this sample, formed due to the immiscibility of a silicate and a sulfide melt (Fig. 5.6d). This is interpreted as to occur during pseudotachylyte formation (Magloughlin 2005). They also represent sites of preferred nucleation of newly crystallized lasts. The microprobe bulk analysis of this sample resulted in a mixture of amphibole and plagioclase comprising the groundmass. According to the microprobe analysis, the lasts are most likely amphibole.
Sample J96-2 represents a sample from the vicinity of sample J96-1 showing comparable macroscopic and microscopic structures (Figs. 5.5e, 5.6e). Here, the individual lasts are a little bit coarser grained (individual dendritical needles up to 100 μm in length). Therefore, the structures indicating initial growth from a melt phase (dendrites, spherolites) are best visible. Microprobe bulk composition points to a mixture of feldspar and amphibole as well.

One fact has to be mentioned. Due to the ultra fine grained texture of the groundmass, the analysed bulk composition could reflect the incorporation of other minerals beside amphibole and feldspar, such as biotite. But this fact could not be solved due to analytical limitations.

## 5.7. Results

To obtain $^{40}Ar/^{39}Ar$ isotopic data, groundmass grains were heated up with the laser system until total fusion, and the gas was purified and subsequently discharged into the mass spectrometer. There, isotopic ratios were obtained for each gas release step. These data were used to produce isochron and plateau plots, and ages were calculated with the Isoplot/Ex program of Ludwig (1999). Table 1 gives an overview about the ages calculated for each sample.

Sample 1b (Jamtal valley, Figs. 5.2, 5.7a) yielded a total gas age of 78.8 ± 0.1 Ma. For isochron calculation we omitted the first two steps of degassing, because of possible influence of radiogenic Ar loss due to diffusion, which would result in too low ages. Calculating the isochron age with the remaining data points resulted in 78.3 ± 5.3 Ma, which is similar to the total gas age. The inverse isochron age resulted in 94.6 ± 0.4 Ma. A plateau age was not obtained, because individual gas release

a 1b

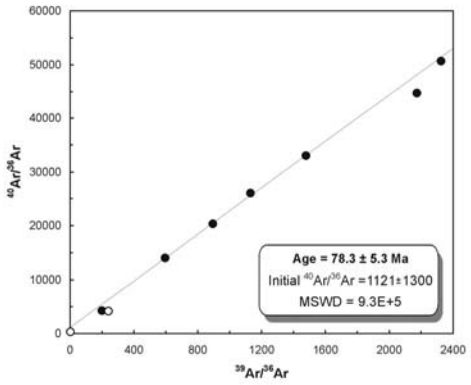
Age = 78.3 ± 5.3 Ma
Initial 40Ar/36Ar =1121±1300
MSWD = 9.3E+5
40Ar/36Ar
39Ar/36Ar

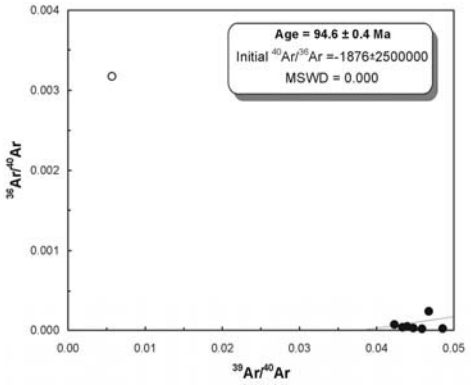
Age = 94.6 ± 0.4 Ma
Initial 40Ar/36Ar =-1876±2500000
MSWD = 0.000
36Ar/40Ar
39Ar/40Ar

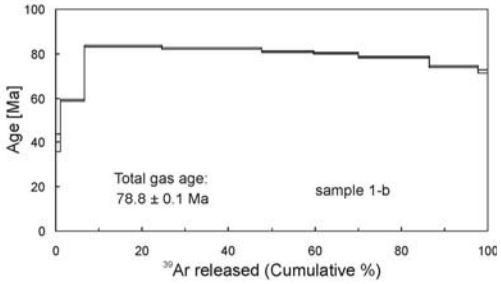
Total gas age:
78.8 ± 0.1 Ma
sample 1-b
Age [Ma]
39Ar released (Cumulative %)

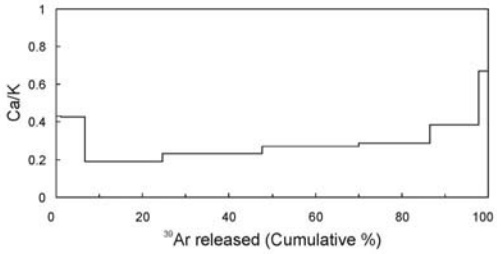
Ca/K
39Ar released (Cumulative %)

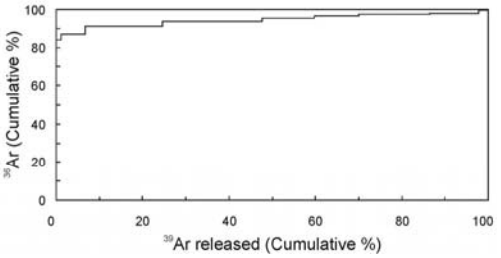
39Ar (Cumulative %)
39Ar released (Cumulative %)

b 5

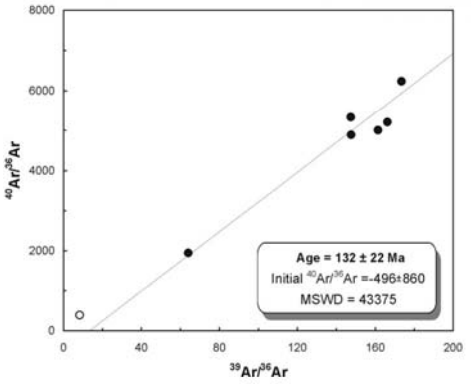
Age = 132 ± 22 Ma
Initial 40Ar/36Ar =-496±860
MSWD = 43375
40Ar/36Ar
39Ar/36Ar

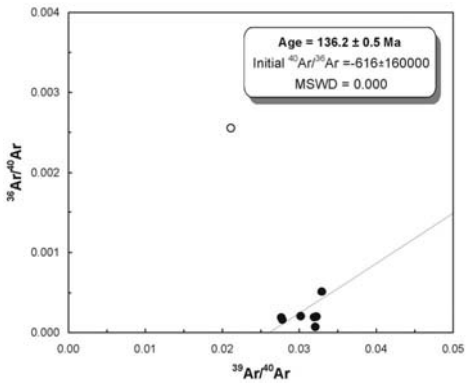
Age = 136.2 ± 0.5 Ma
Initial 40Ar/36Ar =-616±160000
MSWD = 0.000
36Ar/40Ar
39Ar/40Ar

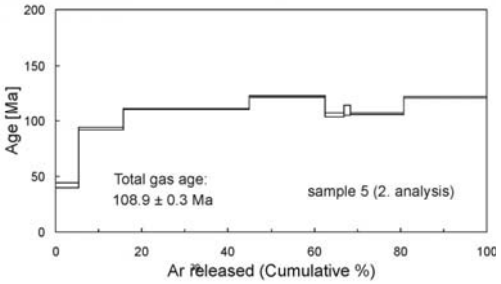
Total gas age:
108.9 ± 0.3 Ma
sample 5 (2. analysis)
Age [Ma]
39Ar released (Cumulative %)

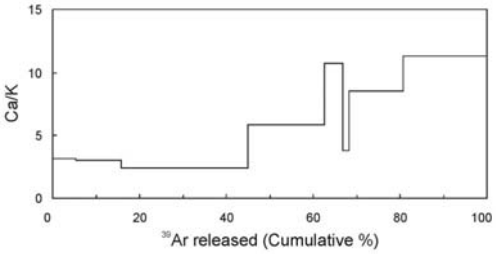
Ca/K
39Ar released (Cumulative %)

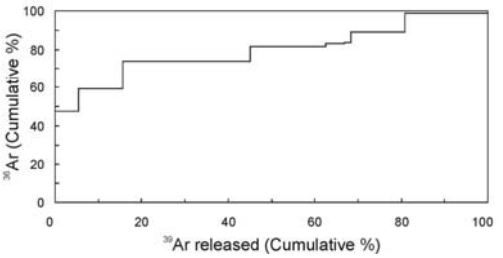
39Ar (Cumulative %)
39Ar released (Cumulative %)

c 16

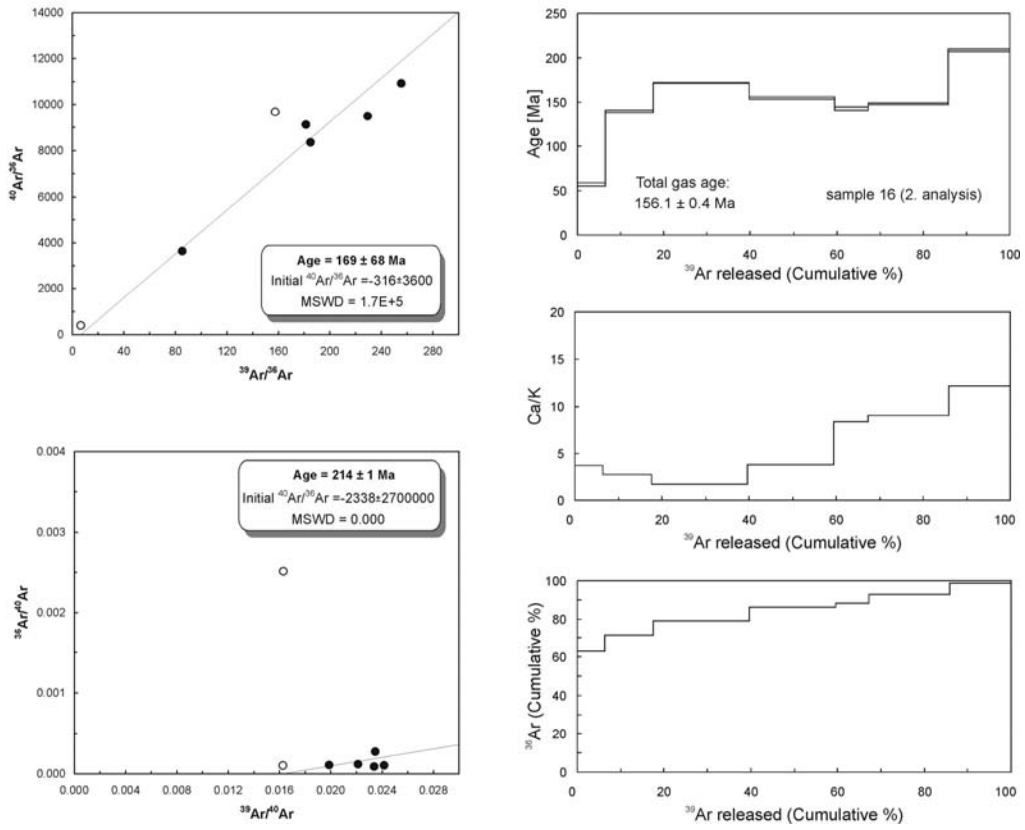
Age = 169 ± 68 Ma
Initial 40Ar/36Ar =-316±3600
MSWD = 1.7E+5
40Ar/36Ar
39Ar/36Ar
Age = 214 ± 1 Ma
Initial 40Ar/36Ar =-2338±2700000
MSWD = 0.000
36Ar/40Ar
39Ar/40Ar
Total gas age:
156.1 ± 0.4 Ma
sample 16 (2. analysis)
Age [Ma]
39Ar released (Cumulative %)
Ca/K
36Ar (Cumulative %)

d J96-1

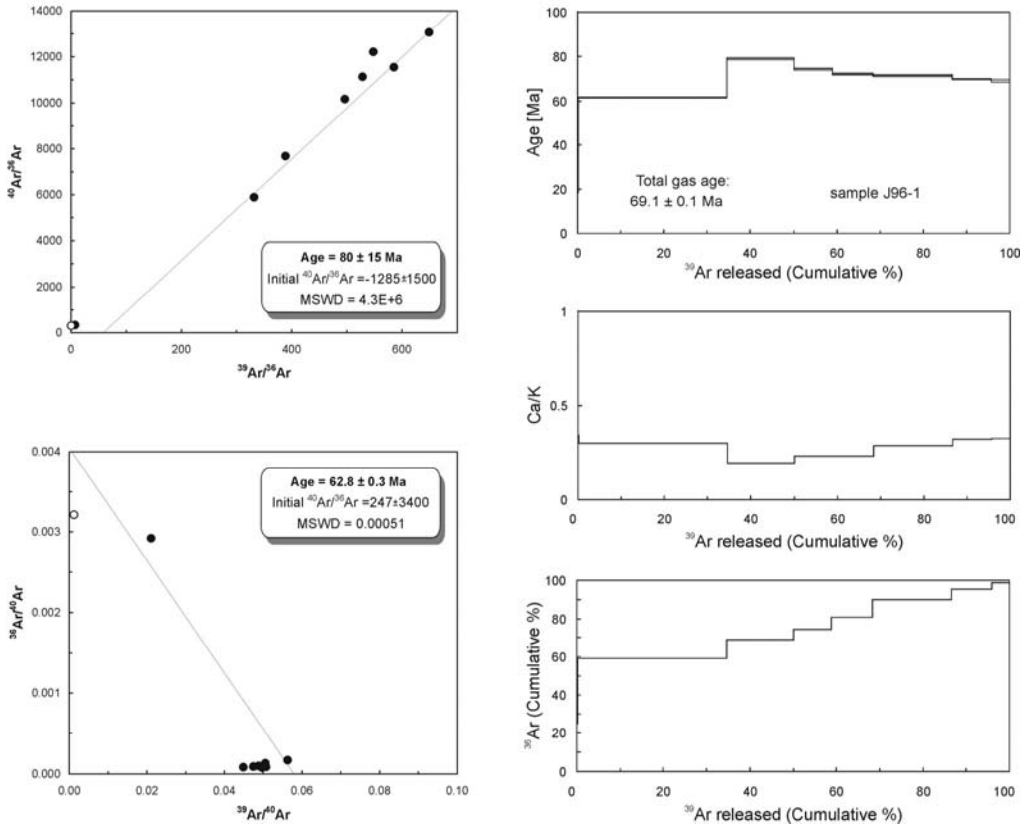
Age = 80 ± 15 Ma
Initial 40Ar/36Ar =-1285±1500
MSWD = 4.3E+6
40Ar/36Ar
39Ar/36Ar
Age = 62.8 ± 0.3 Ma
Initial 40Ar/36Ar =247±3400
MSWD = 0.00051
36Ar/40Ar
39Ar/40Ar
Total gas age:
69.1 ± 0.1 Ma
sample J96-1
Age [Ma]
39Ar released (Cumulative %)
Ca/K
36Ar (Cumulative %)

e J96-1 (2)

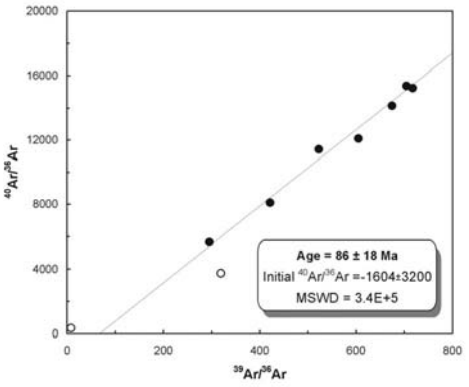


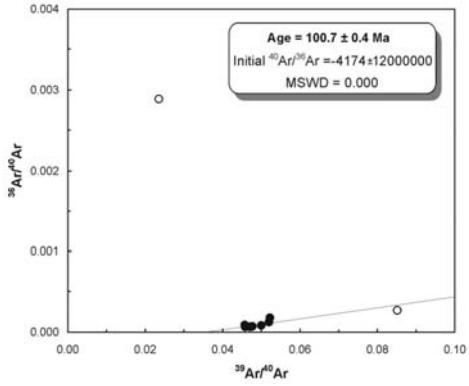


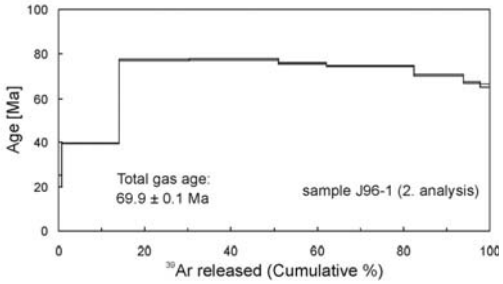


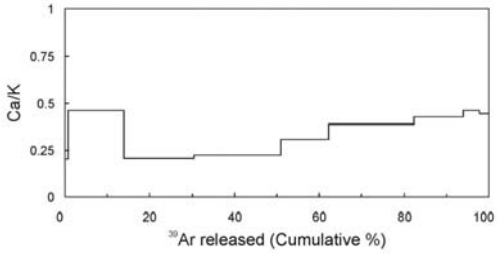


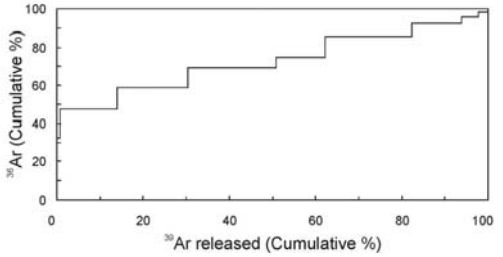


f J96-2

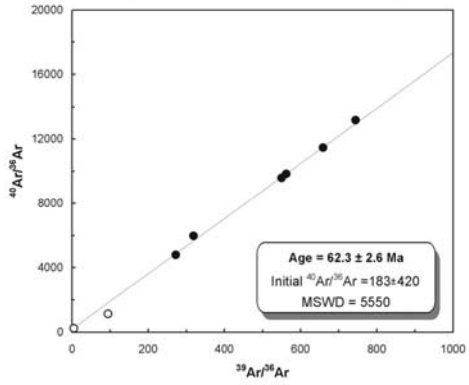


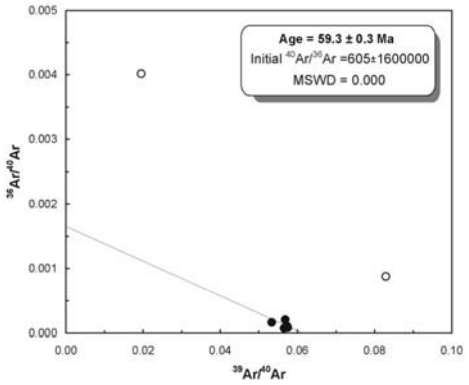


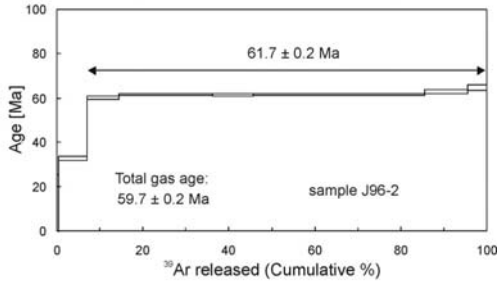


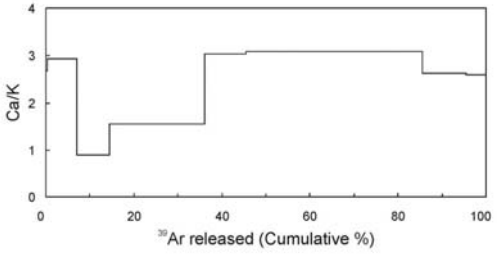


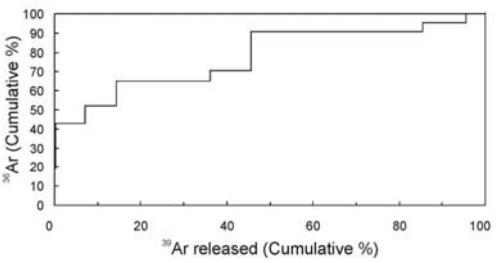

Figure 5.7: Normal isochron, inverse isochron, and plateau diagrams for the analysed samples. Evolution of Ca/K ratios and cumulative Ar release is also given. In addition, different calculated ages are indicated. a) sample 1b, b) sample 5, c) sample 16, d) sample J96-1, e) second measurement of sample J96-1, and f) sample J96-2. See text for details and discussion of data.

steps violated the standards in defining plateau steps (see Chapter 5.5). The Ca/K ratio is quite low, ranging between 0.2 and 0.4. It increases in the last step (total fusion) to roughly 0.7.

Sample 5 (Val Tasna, Figs. 5.2, 5.7b) yielded a total gas age of 108.9 ± 0.3 Ma. We omitted the first gas release step for isochron calculation due to possible excess Ar or Ar loss. The thereby obtained isochron age is 132 ± 22 Ma. The inverse isochron yields an age of 136.2 ± 0.5 Ma. The calculation of a plateau age was not possible for the same reasons as for sample 1b. The Ca/K ratio (between 4 and 11) is slight increased in the last few degassing steps.

Sample 16 (Val Tasna, Figs. 5.2, 5.7c) resulted in a total gas age of 156.1 ±0.4 Ma. We rendered the first and the last degassing steps for isochron calculation due to the individual too low and too high ages, respectively. The normal isochron age resulted in 169 ± 68 Ma. The inverse isochron yields an age of 214 ± 1 Ma. In addition, no plateau age was defined. Ca/K ratios are around 5, increasing to around 10 in the last few steps of Ar release.

Sample J96-1 (Breites Wasser, Figs. 5.2, 6.7d) yielded a total gas age of 69.1 ± 0.1 Ma. Again, the first degassing step was disregarded for isochron calculation due to possible excess or loss Ar. The obtained isochron age is 80 ± 15 Ma. The inverse isochron resulted in 62.8 ± 0.3 Ma. No plateau steps were defined. The Ca/K ratios are generally low around 0.4. In order to check to quality of separation and Ar measurements we conducted a second measurement for the same sample (Fig. 5.7e). This resulted in a total gas age of 69.9 ± 0.1 Ma. We omitted the first two steps in gas release for isochron calculation, which resulted in 86 ± 18 Ma. The inverse isochron age is 100.7 ± 0.4 Ma. No plateau age was obtained. Ca/K ratios are again low, ranging between 0.25 and 0.5.

Sample J96-2 (Breites Wasser, Figs. 5.2, 5.7f) yielded a total gas age of 59.7 ± 0.2 Ma. The first two steps of Ar release were not included into isochron calculation. Normal isochron resulted in an age of 62.3 ± 2.6 Ma. The inverse isochron yielded an age of 59.3 ± 0.3 Ma. Steps 3 to 8 define a plateau. Therefore, the calculated plateau age is 61.7 ± 0.2 Ma. The Ca/K ration is between 1 and 3.

## 5.8. Discussion

Due to the melt origin of pseudotachylytes a resetting of the Ar isotope system is generally expected by degassing of the melt (e.g. Müller et al. 2002). This argues for the use of the $^{40}Ar/^{39}Ar$ isotope system to assess pseudotachylyte generation ages. Potassium bearing phases such as biotite, amphibole, or, to a lesser extend, K-feldspar and low-Ca-plagioclase, are preferentially melted due to their lower melting points (Spray 1992, Müller et al. 2002). Newly crystallized phases would represent the mineralogy of the previously molten paragenesis, also exhibiting K-bearing phases as a prerequisite for the use of the $^{40}Ar/^{39}Ar$ isotope system. This is in accordance with our microprobe bulk analyses of the pseudotachylyte groundmass pointing to a mixture of amphibole, feldspar and possibly biotite, which equal the paragenesis of the host rocks (see Chapter 5.6). As long as the newly formed minerals recrystallized from a completely degassed melt, they do not incorporate initial Ar, and therefore providing correct $^{40}Ar/^{39}Ar$ ages (Müller et

Table 1. Summary of Ar/Ar geochronological data.

| sample | mineral | J value | total gas age [Ma] | isochron age [Ma] | MSWD | inverse isochron age [Ma] | MSWD | plateau age [Ma] | age interpretation [Ma] |
|---|---|---|---|---|---|---|---|---|---|
| *Jamtal valley* | | | | | | | | | |
| 1b | gm | 0.00205 | 78.8 ± 0.1 | 78.3 ± 5.3 | 9.3 E+5 | 94.6 ± 0.4 | 0.00 | no plateau | 78 |
| *Val Tasna* | | | | | | | | | |
| 5 | gm | 0.002049 | 108.9 ± 0.3 | 132 ± 22 | 43375 | 136.2 ± 0.5 | 0.00 | no plateau | > 110 (?) |
| 16 | gm | 0.002049 | 156.1 ± 0.4 | 169 ± 68 | 1.7 E+5 | 214 ± 1 | 0.00 | no plateau | > 150 (?) |
| *Breites Wasser* | | | | | | | | | |
| J96-1 | gm | 0.00205 | 69.1 ± 0.1 | 80 ± 15 | 4.3 E+6 | 62.8 ± 0.3 | 0.01 | no plateau | 65 |
| | gm | 0.00205 | 69.9 ± 0.1 | 86 ± 18 | 3.4 E+5 | 100.7 ± 0.4 | 0.00 | no plateau | 70 |
| J96-2 | gm | 0.00205 | 59.7 ± 0.2 | 62.3 ± 2.6 | 5550 | 59.3 ± 0.3 | 0.00 | 61.7 ± 0.2 | 60 |

gm = groundmass

al. 2002). However, the very short time span expected for frictional melting is supposed to result in only partial isotopic homogenization and the incorporation of inherited $^{40}Ar$ (Müller et al. 2002). This makes the use of the $^{40}Ar/^{39}Ar$ method and the interpretation of the data a quite challenging task.

We tried to omit wall rock fragments and single minerals by the investigation of the 300 µm thick polished slices using a binocular microscope while cutting the pieces for subsequent analyses, as long as they were recognizable at that scale. According to Shimamoto and Nagahama (1992), pseudotachylytes are characterized by the absence of the finest fraction of clasts incorporated within the matrix, when compared to e.g. cataclasites or ultracataclasites. This might be caused by the preferential melting of smaller fragments (e.g. Spray 1992). Therefore, our approach to omit visible fragments might be appropriate to render most of the inherited and distracting clasts. Otherwise, the BSE and SE images obtained with the microprobe and SEM show small newly crystallized lasts, and older fragments (in the range of a few tens of µm), which act as nucleation sites. In consequence, we cannot argue for a complete leave out of wall rock fragments and single crystals. They provide a source for inherited $^{40}Ar$, complicating the interpretation of the obtained isotopic data.

The use of a laser system in order to degas Ar results in a rather localized heating of the sample. Despite of the small spot size, we expect the degassing of Ar to occur from a mixture of the ultra fine grained newly crystallized lasts of possible amphibole, feldspar, and biotite, as well as from wall rock fragments and single crystals, rather than from a homogeneous solidified melt. Therefore, the source for the degassed Ar cannot be tightly constrained, providing an additional error source for analyses. In consequence, the assessment of the potassium content and the thereby constrained minimum weight of the sample to obtain an ample amount of degassed Ar and therefore reliable age results are complicated, if not completely impossible. This might be an additional cause for the badly constrained plateau plots, which failed to produce plateau ages in most cases. In addition, the discrepancy between the different isochron ages and the total gas ages can thereby be explained. In consequence, considering the inhomogeneous texture of the pseudotachylyte matrix, we used the obtained ages to define an "interpreted age" of the individual samples. In addition, the Ca/K ratios provide further hints for the incorporation of wall rock fragments,

which are most likely composed of quartz and feldspar (probably high-Ca-feldspar, e.g. Spray 1992)). As the Ca/K ratio increases for the total fusion step, the incorporation of wall rock fragments is assumed resulting in an apparently too old age for pseudotachylyte generation.

Considering all limitations, we interpreted the age of sample 1b to be roughly 78 Ma due to the similarity of the total gas and normal isochron ages. We excluded the inverse isochron age, because of the clustering of data points resulting in problems constraining the regression line. Therefore, generation of the pseudotachylyte is assumed at ~ 78 Ma. The development of Ca/K ratios might point to the degassing of Ca bearing phases in the higher temperature steps (probably inherited from the wall rock).
Sample 5 is more difficult to evaluate. The total gas age, and both isochron ages differ, not overlapping within errors. Therefore, we interpret the obtained Ar result to point to an age greater than ~ 109 Ma. If this represents a real pseudotachylyte generation age cannot be confirmed. Ca/K ratios strongly alternate for the analysed steps, which points to the incorporation of Ca phases, probably inherited wall rock fragments or single minerals. Microprobe bulk analyses resulted in an elevated Ca content as well.
For sample 16, all individual calculated ages mismatch. The total gas age and the normal isochron age overlap within errors, which is caused by the large error of the latter. The high Ca/K ratios and their development during stepwise heating might point to the involvement of material from the wall rock, degassed at least in the last few steps. Therefore, we interpret the obtained values to result in an age greater than 150 Ma, probably reflecting an age obtained from a disturbed isotope system, rather than a generation age.
Normal isochron and total gas ages for sample J96-1 overlap within errors. In addition, the inverse isochron is roughly comparable to the total gas age. Ca/K ratios are low and do not differ significantly. The second analysis resulted in comparable values, despite of the older inverse isochron age. In consequence, we interpret an age of ~ 65 Ma for this sample. This might reflect a pseudotachylyte generation age.
The best values were obtained for sample J96-2. Total gas age, normal isochron age, and inverse isochron age overlap within the quite small errors. In addition, a plateau age could be defined, which is in a similar range. Ca/K ratio did not provide a clear hint for the incorporation of material from the host rock. Therefore, we interpret that this sample reflects pseudotachylyte generation at roughly 60 Ma.
The Ca/K ratios for samples, from which we obtained the most reliable pseudotachylyte generation ages are much lower than from the samples without a meaningful age. Therefore, monitoring the Ca/K ratio provide an additional hint for the reliability of the obtained ages in terms of possible incorporation of host rock material, both rock fragments and single minerals.

Finally, our obtained $^{40}Ar/^{39}Ar$ ages, as erroneous they might be, point to unstable slip and therewith associated pseudotachylyte formation within the basal parts of the Austroalpine nappe stack during a prolonged time span between 60 Ma to roughly 80 Ma. The data of Thöni (1981, 1988) fall into the bracketed time frame. During that time, South Penninic oceanic crust was subducted underneath the Austroalpine upper plate.

## 5.9. Conclusion

In the here presented study we show $^{40}Ar/^{39}Ar$ ages obtained by stepwise heating using a laser system, which constrain the generation of pseudotachylytes within the basal parts of the Austroalpine nappe stack at the

northwestern rim of the Engadine window. Samples were gained directly above the main thrust plane, where the Austroalpine overrides the South Penninic domain. This occurred during the subduction of the South Penninic ocean underneath the Austroalpine upper plate in the Late Cretaceous to the Eocene.

The heterogeneous texture of the ultra fine grained pseudotachylyte groundmass, most likely composed of a mixture of amphibole, feldspar and biotite, as well as the incorporation of host rock material of comparable size (rock fragments and single minerals) complicate the interpretation of the isotopic data. The Ca/K ratio provides first roughly indications for the degassing of material enriched in Ca, most probable the inherited host rock material.

Taking all analytical and sample derived limitations into account, the assessment of the possible pseudotachylyte generation age is feasible; at least a certain time range can be constrained. For our study area, formation of pseudotachylytes as unambiguous evidence for fossil seismicity is dated to have occurred during a time span between 60 Ma to 80 Ma. This equals isotopic ages for the same working area obtained by Thöni (1981, 1988), which point to unstable slip at roughly 75 Ma. Additionally, our age data expand the time window for the occurrence of unstable slip. Due to the temporal similarity between subduction and pseudotachylyte formation, and the fact that the pseudotachylytes occur subparallel (i.e. slightly discordant) to the main thrust, we interpret the generation of pseudotachylytes to be related to unstable slip processes occurring along the plate interface zone during the course of subduction of the South Penninic ocean underneath the Austroalpine upper plate.

According to Müller et al. (2002) our approach ($^{40}Ar/^{39}Ar$ method, stepwise heating with laser ablation) might be the most suitable methodology in dating pseudotachylytes. There, we were able to exclude most of the inherited host rock material. Due to the heterogeneous texture of the pseudotachylyte matrix (mixture of different recrystallized minerals, host rock fragments, inherited host rock single crystals) the approach of Thöni (1981, 1988) using whole rock material for K/Ar analyses or thin slabs of pseudotachylyte material for Rb/Sr analyses (which is sensu stricto also a whole rock approach) might be erroneous, because of including inherited material to different and undetermined amounts. Nevertheless, his results are comparable to our results, making K/Ar and Rb/Sr a possible option for dating pseudotachylytes as well. However, the dating of pseudotachylytes will remain challenging and erroneous due to the texture of the solidified, and, in most cases, recrystallized melt veins.